RESEARCH ARTICLE

For. Sci. XX(XX):1–14
doi: 10.1093/forsci/fxaa008

biometrics

Population and Stand-Level Inference in Forest Inventory with Penalized Splines

Steen Magnussen, Anne-Sophie Stelzer, and Gerald Kändler

Penalized splines have potential to decrease estimates of variance in forest inventories with a design-based population-level inference, and a model-based domain-level inference by decreasing the likelihood of a model misspecification. We provide examples with second-order (B2) B-splines and radial basis (RB) functions as extensions to a linear working model (WM). Bias was not prominent, yet greater with B2 and in particular with RB than with WM, and decreased with sample size. Important reductions in the variance of a population mean were achieved with both B2 and RB, but at the domain-level only with RB. The proposed regression estimator of variance generated estimates of variance being slightly smaller than the observed variance. A consistent and larger underestimation was seen with the popular difference estimator of variance.

Study Implications: Forest inventories supported by light detection and range (LiDAR) data require—in the estimation phase—a model for linking LiDAR metrics to attributes of interest. Formulating a parametric model can be a challenge and unsatisfactory if the goodness of fit varies across the range of the attribute of interest. A semiparametric model provides more flexibility and lessens the chance of a model misspecification, albeit with the potential of overfitting. A penalty directed at reducing overfitting is required. A flexible semiparametric model is potentially also better suited for applications to small areas like stands than a parametric model. We demonstrate that important reductions in variance are indeed possible, but also that they depend on the form of the nonparametric part of the chosen model and the level of inference (population versus domains). With regard to practical application, reliable estimates of forest attributes at stand-level are of special interest within the scope of forest-management planning, as silvicultural treatments are always stand-oriented, at least with small-scale forestry under Central European conditions, and stand-related volume (basal area, tree density) belongs to the set of relevant parameters for management decisions regarding harvest and regeneration measures.

Keywords: design-based inference, model-based inference, bias, variance estimators, coverage, B-splines, radial basis function

Forest enterprise inventories employing a probability sampling design commonly have dual objectives of providing estimates of totals (means) for both a population and smaller domains such as forest stands (Lappi 2001, Tomppo 2006, Næsset et al. 2011, Goerndt et al. 2013). Design-based population-level inference with model-assisted (MA) estimators (Särndal et al. 1992) has greatly improved the efficiency of enterprise forest inventories (Næsset et al. 2013, Massey and Mandallaz 2015, Kangas et al. 2016). In practice, however, the number of domains of interest may outstrip the sample size and leave the analyst with no other choice than a model-based (MB) inference for domains (Lehtonen et al. 2005, Lehtonen and Veijanen 2009). It is therefore important that an assisting model in a design-based population-level inference is as flexible as possible in order to capture the relation between the study variable and a set of auxiliary variables throughout the population. No assumption is made that a chosen model is the true model (Lehtonen et al. 2005).

Semi- and nonparametric models are flexible and have gained popularity in forestry applications (Kato et al. 2009, Kublin et al. 2013, Nothdurft 2013, Goga and Ruiz-Gazen 2014), in survey statistics (Montanari and Ranalli 2005, Opsomer and Miller 2007, Goga and Ruiz-Gazen 2014), and in forest inventories (Johnson et al. 2008, Penner et al. 2013, Poggio and Gimona 2013, Massey and Mandallaz 2015, Kangas et al. 2016). The popularity of these intrinsic nonlinear models (Gallant 1987, p. 146) is understandable, as they do not require an analyst to fully specify a preferred model, and they are readily available in popular statistical software programs. Because they are flexible, the risk of a model misspecification is reduced compared to a parametric model (Breidt and Opsomer 2009).

Manuscript received May 29, 2019; accepted March 19, 2020; published online June 23, 2020

Affiliations: *Steen Magnussen (steen.magnussen@canada.ca), Natural Resources Canada, Canadian Forest Service, Victoria, British Columbia. Anne-Sophie Stelzer (anne-sophie.stelzer@forst.bwl.de), Forest Research Institute of Baden-Württemberg (FVA Baden-Württemberg), Wonnhaldestraße 4, 79100 Freiburg, Germany. Gerald Kändler (gerald.kaendler@forst.bwl.de), Forest Research Institute of Baden-Württemberg (FVA Baden-Württemberg), Wonnhaldestraße 4, 79100 Freiburg, Germany.*

Acknowledgments: *Two reviewers and the Associate Editor provided helpful and constructive suggestions for improvements to an earlier version of our manuscript. Their help is greatly appreciated.*

Under design-based inference, the difference estimator (DIFF) of variance (Särndal et al. 1992, 6.3.5) has been proposed for semi- and nonparametric models (Opsomer et al. 2007, McConville and Breidt 2013, Breidt and Opsomer 2017). However, in simulations with residuals from nonlinear models fitted to sample data (i.e., the model is internal [Mandallaz et al. 2013]), the difference estimator tends to underestimate the actual variance (Tipton et al. 2013, Massey and Mandallaz 2015, Kangas et al. 2016). The problem of underestimating variance is also known in model-dependent inference (Carter and Eagleson 1992, McRoberts et al. 2018).

In this study, we propose an alternative to the design-based difference estimator of variance in a population mean (or total) in settings where an internal semiparametric model is employed. The proposed estimator is the regression estimator (REG) (Särndal et al. 1992, 6.6.4). We demonstrate the difference estimator and the proposed estimator in two case studies in which a linear assisting model is extended with either B-spline or radial (spline) basis functions (Fahrmeir et al. 2013) designed to capture presumed, but difficult-to-define, nonlinear effects and interactions among predictors in a linear model. Both types of basis functions have gained popularity in natural-resource surveys (Kato et al. 2009, Nothdurft 2013, Goga and Ruiz-Gazen 2014).

The anticipated improvement from using a regression estimator of variance instead of a difference estimator hinges on (1) calibrating the sample means of the auxiliary variables to the known population means and (2) an effective linearization of the model (Särndal et al. 1992, ch. 5.5). Models that include spline functions automatically satisfy the second criterion, as they can be expressed in the scope of a linear model with a set of explanatory variables plus a sum of contributions from "knots" strategically placed in the space of a second set of variables (akin to random effects in a mixed linear model) (Opsomer et al. 2008).

We emphasize that a design-based inference with internal semiparametric models also demands a design-consistent cross-validation for the choice of a smoothing bandwidth, and a constraint in the form of a penalty to control bias (Opsomer and Miller 2007, Breidt and Opsomer 2017, McConville et al. 2017).

The two case studies use data representing forests with a stand structure. Although our primary objective relates to the estimation of a population mean of stem volume density and its variance, a secondary objective is a model-dependent prediction of stand means of this attribute. Here, we explore whether the anticipated efficiency of a semiparametric model at the population level extends to small-area estimation problems (Corona et al. 2014, Ranalli et al. 2016, Wagner et al. 2017).

Material and Methods

For a fixed population—surveyed with a probability sampling design—and composed of N equal area units and M domains, we compare population- and domain-level estimates derived from three unit-level (internal) models for linking a suite of auxiliary variables ($\mathbf{X}$) to a study variable of interest (Y). The auxiliary variables are known for all N units in the population, but Y is known only for the units in a realized sample of size n. For each unit in the population, its sample inclusion probability π_{ij}, $i = 1, \ldots, M$, $j = 1, \ldots, N_i$ is determined according to a probability sampling design that does not recognize domains.

The estimators we consider are for means, variances, and 95 percent confidence intervals for the true mean under simple random sampling without replacement (SI). Domains are forest stands.

Models

The first assisting model in Equation 1 is a parsimonious linear working model (WM) with a structure derived from subject knowledge (Särndal et al. 1992, p. 227):

$$y_{ij} = \mathbf{x}_{ij}\beta'_{\mathrm{WM}} + d_i + e_{ij},\ i = 1,\ \ldots, M,\ j = 1,\ \ldots,\ m_i \quad (1)$$

where y_{ij} is the value of Y in the jth unit of the ith domain, $\mathbf{x}_{ij}$ is a row vector of p_{WM} auxiliary variables, β_{WM} is a row vector of p_{WM} regression coefficients to be estimated from sample data (i.e., the fitted model is internal), d_i is a random effect for the ith domain, and e_{ij} is a model residual error for the jth unit in the ith domain. A transpose of a vector or matrix θ is set as θ'. In our design-based population-level inference under SI, the terms d_i and e_{ij} in Equation 1 are pooled to a single residual error inasmuch as an SI design does not afford a design-consistent estimation of domain effects. When we shift to inference for domains, both d_i and e_{ij} are considered, with d_i regarded as a Gaussian random domain effect with an expectation of zero and a variance σ^2_d, and the residual errors e_{ij} are assumed Gaussian in distribution with an expectation of zero and a variance σ^2_e.

The second (second-order [B2]) and third (radial basis [RB]) models are assisting models that can capture nonlinear effects and nonlinear interactions in auxiliary variables. In the interest of comparing performance, all three models use the same basic set of p_{WM} auxiliary variables. On account of brevity, the nonlinear effects and interactions are limited to two of the auxiliary variables in the WM in Equation 1, say x_1 and x_2. Model B2 can capture separate nonlinear effects in x_1 and x_2, whereas model RB also captures their interactions.

We obtain B2 after first dropping x_1 and x_2 from the WM and then adding a sum over K weighted B2 spline basis functions of x_1 and x_2 (Fahrmeir et al. 2013, p. 426). To wit:

$$y_{ij} = \mathbf{x}_{ij}\beta'_{\mathrm{B2}} + \sum_{q=1}^{2}\sum_{k=1}^{K_{\mathrm{B2}}} \gamma^{\mathrm{B2}}_{qk}\mathrm{B2}_k\left(x_{qij}\right) + d_i + e_{ij},$$
$$i = 1,\ \ldots,\ M,\ j = 1,\ \ldots,\ m_i \quad (2)$$

where $\mathbf{x}_{ij}$is a row vector of $p_{B2} = p_{\mathrm{WM}} - 2$ auxiliary variables, β_{B2} is a row vector of p_{B2} regression coefficients, and $\gamma^{\mathrm{B2}}_{qk}$ is the weight assigned to the kth B2 basis function evaluated at x_{qij} and at a set of Γ_{B2} equally spaced "knots" within the range of x_q, $q = 1,\ 2$; remaining symbols are as in Equation 1 with the caveat that both d_i and e_{ij} are conditional on the model specification(s). The auxiliary variables used in the B-spline extensions of the WM in Equation 1 are identified prior to observing the sample. The number of basis functions K_{B2} is equal to $\Gamma_{\mathrm{B2}} + r - 1$ for each of the two auxiliary variables, where r is the order of the splines (here $r = 2$). As written, B2 is linear in the basis functions.

The evaluation of a B2 basis function at a value z of a single explanatory variable is obtained from lower-order B-spline basis functions as in the following recursive scheme (Fahrmeir et al. 2013, pp. 427–429):

$$
\begin{aligned}
\mathrm{B2}_k(z) &= \frac{z-\kappa_{k-2}}{\kappa_k-\kappa_{k-2}}\mathrm{B1}_{k-1}(z)+\frac{\kappa_{k+2}-z}{\kappa_{k+1}-\kappa_{k+1-2}}\mathrm{B1}_k(z);\\
\mathrm{B1}_k(z) &= \frac{z-\kappa_{k-1}}{\kappa_k-\kappa_{k-1}}\mathrm{B0}_{k-1}(z)+\frac{\kappa_{k+1}-z}{\kappa_{k+1}-\kappa_k}\mathrm{B0}_k(z);\\
\mathrm{B0}_k(z) &= \delta_{\kappa_k\le z<\kappa_{k+1}};\quad \mathrm{B0}_{k-1}(z)=\delta_{\kappa_{k-1}\le z<\kappa_k}
\end{aligned}
\tag{3}
$$

where δ_A is a binary indicator variable taking the value 1 when event A is true, and 0 otherwise. Hence, in applications with second-order B-splines, an addition of $2\times 2=4$ knots outside the range of x_{qij} is needed (q = 1, 2). They are placed symmetrically to the left (right) of the minimum (maximum) of x_q, $q=1,\ 2$. In words, the kth B2 spline basis function between knots κ_{k-1} and κ_{k+1} is a "bell-curve" with a maximum value of 0.75 at κ_k and zero for all values less than κ_{k-1} and greater than or equal to κ_{k+1}. The sum over the full set of B-spline basis functions evaluated at a point z is always 1.0.

The RB model is designed to capture not only nonlinear effects in x_1 and x_2, but also potential nonlinear interactions. As for the B2 model, this is achieved by again dropping x_1 and x_2 from the WM in Equation 1, but now adding a sum over a set of K_{RB} weighted RB functions of x_1 and x_2. We get

$$
y_{ij}=\mathbf{x}_{ij}\beta'_{\mathrm{RB}}+\sum_{k=1}^{K_{\mathrm{RB}}}\gamma_k^{\mathrm{RB}}\mathrm{RB}_k\left(x_{1ij},x_{2ij}\right)+d_i+e_{ij},\quad i=1,\ \ldots,\ M,\ j=1,\ \ldots,\ m_i \tag{4}
$$

where $\mathbf{x}_{ij}$is a row vector of $p_{\mathrm{RB}}=p_{\mathrm{WM}}-2$ auxiliary variables, β_{RB} is a row vector of p_{RB} regression coefficients, and γ_k^{RB} is the weight assigned to the kth RB function evaluated at $\left(x_{1ij},\ x_{2ij}\right)$ and a set Γ_{RB} of K_{RB} bivariate "knots" $(\kappa_1,\ \kappa_2)$ with maximum separation within the space spanned by $\left(x_{1ij},\ x_{2ij}\right)$ (Lister and Scott 2009, Bia and Van Kerm 2014); remaining symbols are as in Equation 1.

The RB functions used here are those recommended by Ruppert et al. (2003), as they provide for a low rank smoothing akin to kriging, and a first-order approximation to thin plate spline smoothing (Boer et al. 2001). Briefly,

$$
\mathrm{RB}_k\left(x_{1ij},\ x_{2ij}\right)=\left\|\left(x_{1ij},\ x_{2ij}\right)-\left(\kappa_{1k},\ \kappa_{2k}\right)\right\|^2\log\left(\left\|\left(x_{1ij},\ x_{2ij}\right)-\left(\kappa_{1k},\ \kappa_{2k}\right)\right\|\right)_{\boldsymbol{\Omega}^{-0.5}_{\kappa_{1k},\ \kappa_{2k}}} \tag{5}
$$

with

$$
\boldsymbol{\Omega}=\begin{pmatrix}\mathrm{RB}_1\left(\kappa_{11},\ \kappa_{21}\right) & \cdots & \mathrm{RB}_1\left(\kappa_{11},\ \kappa_{2K_{\mathrm{RB}}}\right)\\ \vdots & \ddots & \vdots\\ \mathrm{RB}_1\left(\kappa_{1K_{\mathrm{RB}}},\ \kappa_{21}\right) & \cdots & \mathrm{RB}_1\left(\kappa_{1K_{\mathrm{RB}}},\ \kappa_{2K_{\mathrm{RB}}}\right)\end{pmatrix} \tag{6}
$$

where $\|\mathbf{s}\|$ denotes the Euclidean length (norm) of a vector $\mathbf{s}$, and $\boldsymbol{\Omega}^{-0.5}_{\kappa_{1k},\ \kappa_{2k}}$ is the element in row κ_{1k} and column κ_{2k} in the inverse of the matrix square root of the $K_{\mathrm{RB}}\times K_{\mathrm{RB}}$ symmetric matrix $\boldsymbol{\Omega}$ (Johnson et al. 2001). By definition, for a distance of zero, an RB function takes the value of 1 (Ruppert et al. 2003, p. 244). For a given input $\left(x_{1ij},\ x_{2ij}\right)$, the output is a set of K_{RB} weights to the "knots" in the space of the input variables.

RB functions may be extended to three and higher dimensions (Buhmann 2003), but in dimensions higher than two, the covariance matrix $\boldsymbol{\Omega}$ may not be non-negative definite (Chilès and Delfiner 1999, p. 187).

Parameter Estimation

Estimates of the WM regression coefficient vector β_{WM} in Equation 1 were obtained via the method of weighted least squares (Draper and Smith 1998, p. 108) using the inverse of the sample inclusion probability of unit ij $\left(\pi_{ij}\right)$ as weight (Särndal et al. 1992, 6.4.2).

Estimates of the B2 and RB regression coefficients β and γ in models 2 and 4 were obtained via weighted penalized least squares (PLS, Fahrmeir et al. 2013, ch. 8.1.3). Let $\mathbf{z}_{ij}$ denote a concatenation of the vectors of the unit-level predictors in models B2 and RB, respectively; let $\mathbf{Z}$ note the matrix with n rows of the concatenated vectors $\mathbf{z}_{ij}$, and let θ denote the concatenation of the regression coefficients to $\mathbf{z}_{ij}$. The PLS estimate of θ, with a design-based cross-validation choice of smoothing (λ), was obtained by minimizing a model assisted estimator of variance (Opsomer and Miller 2007, Equation 9) with respect to λ

$$
V_{\mathrm{cv}}(\lambda)=\sum\nolimits_{ij\ni s}\frac{\pi_{ij}-\pi_i\pi_j}{\pi_{ij}}\frac{\left(y_{ij}-\mathbf{z}_{ij}\theta'_\lambda\right)}{\pi_i}\frac{\left(y_{ij}-\mathbf{z}_{ij}\theta'_\lambda\right)}{\pi_j} \tag{7}
$$

where θ'_λ is a penalized least-squares estimate of θ that depends on λ and the choice of penalty. Specifically, the estimate θ'_λ satisfies $\mathbf{Z}\theta'_\lambda=\mathbf{S}_\lambda^{(-)}\mathbf{y}$ where $\mathbf{y}$ is a length n row vector of observations of Y, and $\mathbf{S}_\lambda^{(-)}$ is a design-based version of a penalized least-squares smoothing matrix obtained after a modification of a conventional PLS smoothing matrix $\mathbf{S}$ (Fahrmeir et al. 2013, p. 469). We have

$$
\mathbf{S}_\lambda^{(-)}=\frac{\mathbf{S}-\mathrm{Diag}(\mathbf{S})}{\mathbf{J}_{n\times n}-\mathbf{J}_{n\times n}\mathrm{Diag}(\mathbf{S})},\ \text{with}\ \mathbf{S}=\mathbf{Z}(\mathbf{Z}'\mathbf{Z}+\lambda\mathbf{D}+\ \upsilon\ \mathbf{I})^{-1}\mathbf{Z}' \tag{8}
$$

where $\mathbf{J}_{n\times n}$ is an $n\times n$ matrix of ones, and $\mathbf{D}$ is a second-order difference penalty matrix (Fahrmeir et al. 2013, p. 437) with the first $p_{\mathrm{B2}}=p_{\mathrm{RB}}$ rows and columns equal to 0, as no penalty is leveraged against the $p_{\mathrm{WM}}-2$ regression coefficients in β_{B2} and β_{RB}, and υ is a small term to ensure the existence of the inverse (Opsomer and Miller 2007, Equation 5). Here we take υ as $1/N$. The remaining submatrix of $\mathbf{D}$ is five-banded (Golub and Van Loan 2012, ch. 4.3) with elements {1, 5, 6, 6, …, 6, 6, 5, 1} along the main diagonal (band 0), {–2, –4, –4, … –4, –4, –2} along bands (subdiagonals) ±1, and {1, 1, …, 1, 1} along bands ±2. For the λ that minimizes Equation 7, the sample-based and design-consistent PLS solution becomes (Fahrmeir et al. 2013, 8.3)

$$
\hat{\theta}=\left(\boldsymbol{Z}'\boldsymbol{\Pi}^{-1}\boldsymbol{Z}+\lambda\boldsymbol{D}+\ \upsilon\ \boldsymbol{I}\right)^{-1}\boldsymbol{Z}'\boldsymbol{\Pi}^{-1}\boldsymbol{y} \tag{9}
$$

where $\mathbf{Z}$ is the matrix of sample values of the predictors, $\boldsymbol{y}$ is the vector of sample values of Y, and $\boldsymbol{\Pi}$ is an $n\times n$ diagonal matrix of sample inclusion probabilities. The penalty term was estimated via a grid search of candidate values for λ followed by a second-order interpolation to find the value of λ that minimizes Equation 7, and subsequently we used this value to obtain $\hat{\boldsymbol{\theta}}$ as per Equation 9.

For the domain-level inference, the above parameters were re-estimated after ignoring the sample inclusion probabilities (the design) (Mandallaz 2008, p. 49). For our equal probability (SI) design, this is without consequence. To compute the variance of a domain mean (cf. below), we also need to decompose the residual variance to an among-domain variance σ_d^2 and a within-domain variance σ_e^2. Estimates of these variance components were obtained using Henderson's method III (Searle et al. 1992, ch. 5.5) for unbalanced data, which uses moment estimators. Preliminary analyses had shown that this method was more robust than the more popular empirical best linear unbiased prediction estimator (Pinheiro and Bates 2000, ch. 4).

Estimators for Population-Level Inference

In accordance with our objective of assessing the regression estimator of variance as an alternative to the difference estimator of variance when a semiparametric model is internal, i.e., fitted to sample data, we next present both estimators.

The model assisted regression estimator of a population mean of Y can be written as a weighted ("g-weights") linear function of the π-expanded sample values of Y: (Särndal et al. 1992, 6.5.9)

$$\hat{\bar{y}}^{\mathrm{REG}}_{\mathrm{MOD}} = N^{-1}\sum_{ij\in s}\hat{g}^{\mathrm{MOD}}_{ij}y_{ij}\pi^{-1}_{ij},\ \mathrm{MOD} = \mathrm{WM},\ \ \mathrm{B2},\ \ \mathrm{RB}$$
$$\text{with } \hat{g}^{\mathrm{MOD}}_{ij} = 1 + (\mathbf{t_z} - \hat{\mathbf{t}}_{\mathbf{z}})'\hat{\mathbf{T}}^{-1}\mathbf{z}'_{ij} \tag{10}$$

where g^{MOD}_{ij} is a design-based weight given to y_{ij}, $\mathbf{t}_z$ is the true population total of the vector of predictors, $\hat{\mathbf{t}}_{\mathbf{z}}$ is the design-based estimate of this total, and $\hat{\mathbf{T}}$ is the matrix of sample sums of cross-products $\mathbf{z}'_{ij}\mathbf{z}_{ij}\pi^{-1}_{ij}$ (Särndal et al. 1992, 6.4.11). The notation $ij \in s$ indicates that unit ij is in the observed sample.

Under an SI design, the difference estimator—with the $(\mathbf{z}_{ij}, \theta)$ notation used in Equation 7 and for a population mean of Y—can be written as (Särndal et al. 1992, 6.3.4)

$$\hat{\bar{y}}^{\mathrm{DIF}}_{\mathrm{MOD}} = \hat{\boldsymbol{\theta}}'_{\mathrm{MOD}}\bar{z} + N^{-1}\sum_{ij\in s}\pi^{-1}_{ij}\left(y_{ij} - \hat{y}_{ij}\right),$$
$$\mathrm{MOD} = \mathrm{WM},\ \mathrm{B2},\ \mathrm{RB} \tag{11}$$

where $\hat{\boldsymbol{\theta}}'_{\mathrm{MOD}}$, in the case of the WM model, is the weighted least-squares estimate of β_{WM}, $\bar{z}$ is the (known) population mean of the auxiliary variables, and $\hat{y}_{ij}$ is the marginal prediction of y_{ij} conditional on the estimated regression coefficients. Note that for WM, the estimators in Equations 10 and 11 are equal.

With the RB model, we occasionally encountered negative g-weights. In those cases with negative projections of T in Equation 10 onto the real line, T was subject to a single value decomposition (SVD, Searle 1982, pp. 209 and 316) with the eigenvalues less than 10^{-8} times the largest eigenvalue of T set to zero. If the reconstructed T matrix with these new eigenvalues continued to produce negative g-weights, the SVD was iterated until all g-weights became positive. Between one and six iterations sufficed in most cases.

The variance estimator of $\hat{\bar{y}}^{\mathrm{REG}}_{\mathrm{MOD}}$ (Särndal et al. 1992, 6.6.4) is

$$\hat{V}\left(\hat{\bar{y}}^{\mathrm{REG}}_{\mathrm{MOD}}\right) = N^{-2}\sum_{ij\ni s}\sum_{uv\ni s}\breve{\Delta}_{ij,uv}\left(\hat{g}^{\mathrm{MOD}}_{ij}\breve{e}_{ij}\right)\left(\hat{g}^{\mathrm{MOD}}_{uv}\breve{e}_{uv}\right),$$
$$\mathrm{MOD} = \mathrm{WM, B2, RB} \tag{12}$$

where $\breve{e}_{ij}$ is the π-expanded regression residual $\left(y_{ij} - \hat{y}_{ij}\right)\pi^{-1}_{ij}$, and $\breve{\Delta}_{ij,uv}$ is the π-expanded joint sample inclusion probability of units ij and uv $\left(\breve{\Delta}_{ij,\,uv} = 1 - \pi_{ij}\pi_{uv}\pi^{-1}_{ij,uv} \text{ for } ij \neq uv,\ \breve{\Delta}_{ij,ij} = 1 - \pi_{ij}\right)$.

It became clear that the g-weights for RB computed following an SVD decomposition generated a lower variance estimate than without the SVD decomposition. To counter this unintended side-effect, we multiplied $\hat{V}\left(\hat{\bar{y}}^{\mathrm{REG}}_{\mathrm{MOD}}\right)$ by a correction factor C^2_{RB} with $C_{\mathrm{RB}} = \sum_{ij\in s}\left|\tilde{g}^{\mathrm{RB}}_{ij}\right| / \sum_{ij\in s}\left|\hat{g}^{\mathrm{RB}}_{ij}\right|$ where $\left|\tilde{g}^{\mathrm{RB}}_{ij}\right|$ is the absolute of the g-weight estimated prior to the SVD decomposition.

The difference estimator of variance (Särndal et al. 1992, 6.3.6) is

$$\hat{V}\left(\hat{\bar{y}}^{\mathrm{DIF}}_{\mathrm{MOD}}\right) = N^{-2}\sum_{ij\ni s}\sum_{uv\ni s}\breve{\Delta}_{ij,uv}\breve{e}_{ij}\breve{e}_{uv}, \mathrm{MOD} = \mathrm{WM,B2,RB} \tag{13}$$

Nominal 95 percent normal confidence intervals for the population mean $\bar{y}$ were computed as $\hat{\bar{y}}^{\mathrm{EST}}_{\mathrm{MOD}} \pm 1.96\sqrt{\hat{V}\left(\hat{\bar{y}}^{\mathrm{EST}}_{\mathrm{MOD}}\right)}$, MOD = WM, B2, RB, EST = REG, DIFF.

In the simulated case study with $\bar{y}$ known, we computed the proportion of 1,000 intervals (viz. coverage) that contained the actual population mean $\bar{y}$ (Särndal et al. 1992, p. 534, Rao and Hidiroglou 2003).

Estimators for Domain-Level Inference

For domain i with $i = 1, \ldots, M$, the MB estimator of the mean of Y_i is (Chambers and Clark 2012, 7.2 p. 72)

$$\hat{\bar{y}}^{\mathrm{MB}}_{\mathrm{MOD},\ i} = \bar{y}_{s_i} + (N_i - n_i)^{-1}\sum_{j\notin s_i}\mathbf{z}^{\mathrm{MOD}}_{ij}\hat{\boldsymbol{\theta}}'_{\mathrm{MOD}},$$
$$\mathrm{MOD} = \mathrm{WM},\ \mathrm{B2},\ \mathrm{RB} \tag{14}$$

where $\bar{y}_{s_i}$ is the mean of y_{ij} of the sample units located in the ith domain (if any), n_i is the number of units from the ith domain in the sample (s_i), and N_i is the size in units of the ith domain. When n_i is zero, the estimator in Equation 12 becomes regression-synthetic, i.e., purely derived from information external to the ith area, we now rely on the assumption that the population-level model holds in every small area (stand) of interest, which leads to a synthetic method of inference (Chambers and Clark 2012, ch. 15.1). In Equation 14, the use of $\bar{y}_{s_i}$ ensures the most efficient estimator. Dropping $\bar{y}_{s_i}$ and using a facultative summation of model predictions for all units in a small area instead (for example, McRoberts et al. 2013) provides a less efficient estimator, since unbiased information is ignored.

The MB variance estimator for the mean in the ith domain is (Chambers and Clark 2012, 7.4, p. 73)

$$\hat{V}\left(\hat{\bar{y}}^{\mathrm{MB}}_{\mathrm{MOD},\ i}\right) = N_i^{-2}\left(\boldsymbol{t}_{z^{\mathrm{MOD}}_i\setminus s_i}\hat{\boldsymbol{\Sigma}}\left(\hat{\boldsymbol{\theta}}^{\mathrm{MOD}}\right)\boldsymbol{t}'_{z^{\mathrm{MOD}}_i\setminus s_i} + \hat{\sigma}^2_d + (N_i - n_i)\,\hat{\sigma}^2_e\right),$$
$$\mathrm{MOD} = \mathrm{WM},\ \mathrm{B2},\ \mathrm{RB} \tag{15}$$

where $\mathbf{t}_{zi\setminus s_i}$ is the (known) vector of totals for the explanatory variables in the $N_i - n_i$ units of the ith domain *not* in the sample (s_i) from the ith domain. As before, $\hat{\sigma}^2_d$ and $\hat{\sigma}^2_e$ are model-specific and conditional on $\hat{\boldsymbol{\theta}}^{\mathrm{MOD}}$. We obtained nominal 95 percent normal confidence intervals for an estimated domain mean and, in one case, also the coverage of an estimated interval (cf. above).

Case Studies

HUC Forest.

The population is artificial and composed of 21,025 fixed equal area sampling units divided into 112 forest stands (domains) of different size (see Appendix A for details). The study variable is stem volume (VOL; unit: m^3 ha^{-1}), and it is desired to obtain a sample-based estimate of the population mean of VOL and the mean of VOL for each stand. An estimate of uncertainty and a nominal 95 percent confidence interval for the true but unknown mean of VOL is also required. Five unit-level auxiliary variables assumed useful as predictors of VOL are available for every unit in the population: elevation (ELEV; unit: m), mean canopy height (CH; unit: m), standard deviation of canopy height (sCH; unit: m), longitude (LON °W; unit: degree), and latitude (LAT °N; unit: degree). CH and sCH are metrics derived from data captured during a virtual airborne laser scanning of the forest (Wulder et al. 2013). Simulation details are provided in Appendix A.

An equal probability sampling design without replacement (SI) with a sample size n of 200, 300, and 400 units is simulated. Predictors in the WM in Equation 1 are LAT, LON, ELEV, CH, and sCH. The B2 model is linear in the variables ELEV, CH, and sCH, and has a nonlinear second-order B-spline extension in the variables LAT and LON in the form of $K_{B2} = 9$ second-order B-spline basis functions evaluated at LAT_{ij} and LON_{ij} plus a set of eight equally spaced values ("knots") within the ranges, and four "knots" placed symmetrically outside the ranges of LAT and LON, respectively.

The RB model is also linear in ELEV, CH, and sCH, and it has a nonlinear extension with $K_{RB} = 63$ RB functions evaluated at locations (LAT_{ij}, LON_{ij}) and 63 "knot" locations uniformly placed with a maximum of separation within the spatial domain of hydrological unit codes (HUC). The RB functions capture not only nonlinear effects in LAT and LON, but also nonlinear interactions in these variables. The STATA® software algorithm *fillin* by Bia and Van Kerm (2014) was used to place the "knots."

Note, for both B2 and RB, the degrees of freedom (df) expended on the nonparametric part is lower than the number of basis functions (Fahrmeir et al. 2013, p. 474). Specifically, we used df = Trace(2**S**-**SS**′) (Fahrmeir et al. 2013, p. 475) with **S** defined in Equation 8, instead of the more common df = Trace(**S**) because **S** was rarely symmetric. In our HUC simulations, with $n = 200$, an average of 18.6 (±1.9) dfs were used in B2, and 10.9 (±0.3) were used in RB. These numbers increased slightly with sample size, and they were 19.8 (±0.6), and 11.1 (±0.3), respectively with $n = 400$.

We replicated the simulated sampling with the three sample sizes 1,000 times and obtained the above estimators for both the HUC forest and its 112 stands.

Betriebsinventur (BI) Data from Baden-Württemberg.

In this case study (see Appendix B for details), we focused on forest stands in the state forest of the district "Breisgau-Hochschwarzwald" in Baden-Württemberg, Germany, for which data from an image flight were available for the year 2015. We used digital aerial stereo images from the regular aerial surveys of the Baden-Württemberg land-surveying authority (LGL)[1] to generate a digital surface model (DSM). LGL also provided us with a high-quality digital terrain model (DTM) with 1-m resolution. Based on data from the DSM and the DTM, we deduced the normalized DSM (nDSM) which describes the height of off-terrain objects at every position of the survey area. Standardized processes as detailed in Appendix B were applied to acquire the auxiliary information from the stereo image point clouds and from the DTM. The area unit (pixel) for the auxiliary variables was a 20 × 20 m square.

For illustration purposes, we used a subarea with a higher density of forest stands (see Figure 1). This area covers 862 forest stands, representing 4,731 hectares in total, where single stands have a size of 0.2–45.9 hectares with a median size of 3.59 hectares. The auxiliary data were generated for those 118,266 pixels overlapping by at least 50 percent with the selected forest stands. The data from plots of the enterprise inventory BI in 2015 in the state forest served as terrestrial data. A total of 436 forest stands in our study area contained at least one BI plot that was surveyed in 2015, representing an area of 3,080 hectares in total. Overall, 770 BI plots were distributed over these forest stands, whereas at most, seven BI plots were located in one single forest stand. For all of these 436 forest stands, both terrestrial and auxiliary data were available. The remaining 426 forest stands in our study area did not contain any BI plot that was surveyed in 2015. As a result, only auxiliary data were available for these forest stands.

As in the HUC study, the study variable is VOL (unit: m^3 ha^{-1}), and we want to obtain a sample-based estimate of the population mean of VOL and the mean of VOL in each stand (details on this variable can be found in Appendix B). Further, we want to estimate the uncertainty and a 95 percent confidence interval for the mean of VOL. Based on the data from the BI plots, the empirical mean volume for all stands is 432.41 m^3 ha^{-1} with a standard deviation of 231.83 m^3 ha^{-1} and a standard error of 8.35 m^3 ha^{-1}, respectively. The volume ranges between 7.16 m^3 ha^{-1} and 1,620.43 m^3 ha^{-1}, depending on the measurements at the BI plots.

We used the following five unit-level auxiliary variables: total crown coverage (CC; unit: percent), mean CH (unit: m), standard deviation of canopy height (sCH; unit: m), total volume underneath the normalized digital surface model (VolnDSM; unit: m^3 ha^{-1}), and elevation (ELEV; unit: m). ELEV is directly obtained from the DTM, whereas all other metrics are derived from the information deduced from the digital aerial stereo images, partly in combination with the DTM.

We used the same five predictors $\mathbf{x}_{ij}$ in all three models: for the WM in Equation 1, we included CC, CH, sCH, VolnDSM, and ELEV. The linear part of the B2 model in Equation 2 included CC, CH, and sCH, plus a weighted sum of $K_{B2} = 9$ second-order B-spline basis functions evaluated at $VolnDSM_{ij}$, and a weighted sum of $K_{B2} = 9$ second-order B-spline basis functions evaluated at $ELEV_{ij}$. Therefore, we considered a set of eight equally spaced VolnDSM (ELEV) values ("knots") within the range of VolnDSM (ELEV) and four "knots" placed symmetrically outside this range. For the RB model in Equation 4, we also used CC, CH, and sCH as linear explanatory variables ($\mathbf{x}_{ij}$), plus a weighted sum of $K_{RB} = 146$ RB functions evaluated at locations ($VolnDSM_{ij}$, $ELEV_{ij}$). The corresponding 146 "knot" locations are placed by uniformly expanding a grid over a prespecified number of 15 values each for VolnDSM and ELEV, and subsequently clipping according to a convex hull around the data points using R version 3.4.0. Our choice of knots was guided by recommendations in Ruppert et al. (2003, ch. 5.5).

Results

HUC Forest.

Estimates of the mean stem volume density (VOL m^3 ha^{-1}) are listed in Table 1. With the linear WM model, the apparent bias in the REG and DIFF estimators was approximately equal and varied from –0.04 percent (n = 200) to 0.06 percent (n = 400). With the B2 model, the apparent bias in the REG estimator was –0.13 percent (n = 200), which declined to just 0.01 with n = 400. The apparent bias in the DIFF estimator was less (–0.07 percent) with n = 200, but slightly larger (0.02 percent) with n = 400. The RB model generated consistently the largest bias with the REG estimator (from –0.55 percent with n = 300 to –0.35 percent with n = 400) and only slightly less biased results with the DIFF estimator (from –0.31 percent with n = 300, to –0.20 percent with n = 400 percent). We failed to reject the null hypothesis of a zero bias in REG and DIFF estimates of VOL m^3 ha^{-1} (5 percent level) for WM and B2, but rejected, for all sample sizes, the null hypothesis in case of RB. The apparent decrease in bias in B2 and RB with increasing sample size suggests nearly unbiasedness with sample sizes larger than used here.

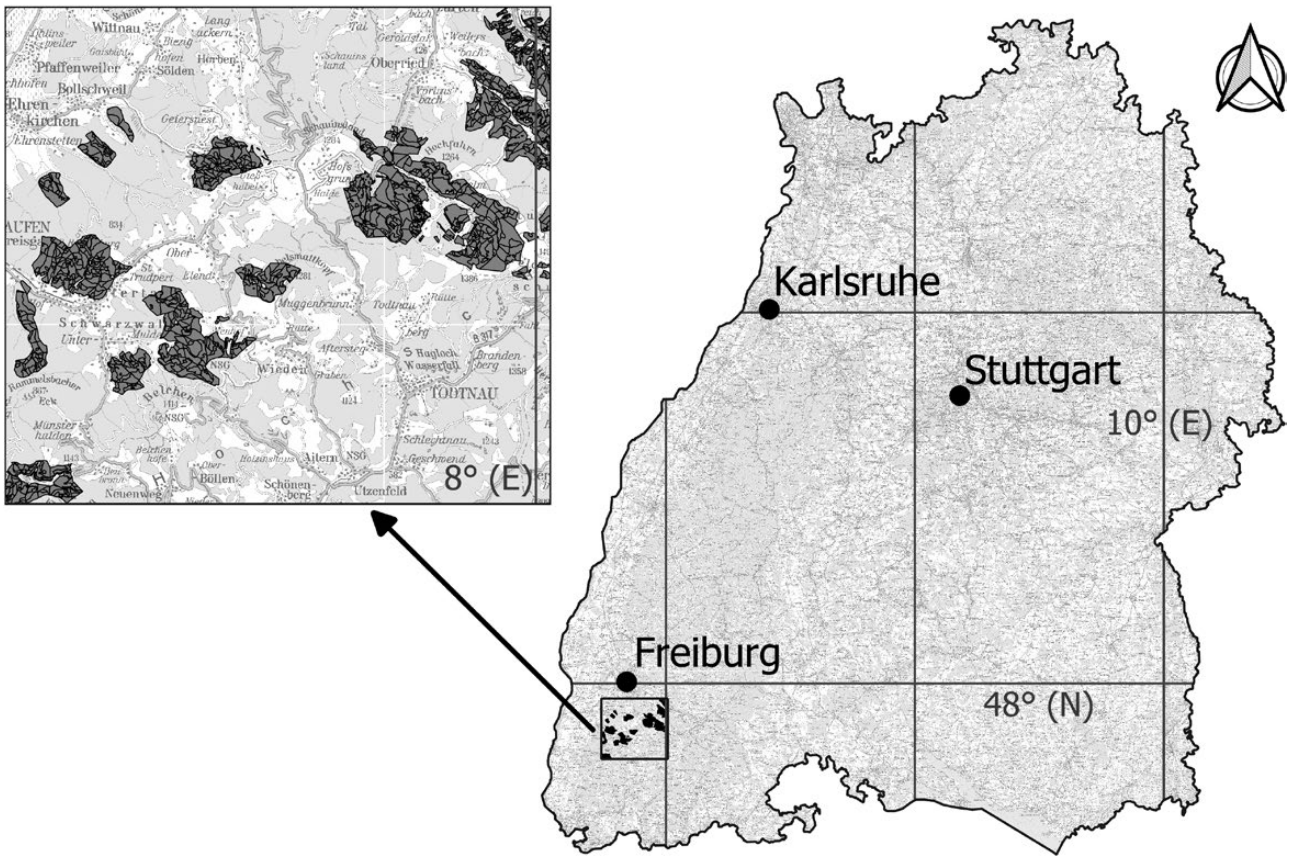

Figure 1. Map of Baden-Württemberg, Germany (right). The callout (left) displays the 862 forest stands in the state forest we focused on in our case study.

Table 1. Estimates of VOL in the HUC forest and associated estimates of relative bias (BIAS percent = BIAS / VOL × 100), eSE, oSE, and COV_{95} of nominal 95 percent confidence intervals.

Sample size		200	200	200	300	300	300	400	400	400
Statistic	Estimator	WM	B2	RB	WM	B2	RB	WM	B2	RB
Mean	REG	404.7	404.4	402.7	405.0	404.9	403.2	405.1	404.9	403.5
	DIFF	404.7	404.6	403.6	405.0	404.9	403.8	405.1	405.0	404.1
BIAS percent	REG	–0.04	–0.13	–0.55	0.02	0.00	–0.43	0.06	0.01	–0.35
	DIFF	–0.04	–0.07	–0.31	0.02	0.01	–0.26	0.06	0.02	–0.20
eSE	REG	15.1	13.0	13.3	12.2	10.5	9.0	10.6	9.1	7.7
	DIFF	14.8	12.2	9.4	12.1	10.1	8.0	10.5	8.8	7.1
oSE	REG	15.5	13.6	13.3	12.6	10.9	10.5	10.9	9.1	7.7
	DIFF	15.5	13.6	13.6	12.6	10.9	10.5	10.9	9.5	8.8
COV_{95}	REG	0.95	0.93	0.92	0.94	0.94	0.90	0.94	0.93	0.91
	DIFF	0.94	0.92	0.81	0.94	0.92	0.84	0.94	0.93	0.88

Note: Analytical standard errors are the square root of the variances in Equations (12) and (13), observed standard errors are the standard deviations across 1,000 replications. Actual mean stem volume is 404.9 m^3 ha^{-1}. COV_{95}, coverage of nominal 95 percent confidence intervals; DIFF, difference estimator; eSE, estimated (analytical) standard error; oSE, empirical standard error; HUC, hydrological unit codes; REG, regression estimator; VOL, mean stem volume density; WM, working model.

Estimated (analytical) standard errors (eSE) are listed in Table 1. All the estimates follow the expected trend of a decline at the rate of $\sqrt{n}$ with increasing sample sizes. Across sample sizes, the lowest REG errors were obtained with RB (mean 10.2 m^3 ha^{-1}), followed by B2 (10.9 m^3 ha^{-1}). The largest error of 12.7 m^3 ha^{-1} was with the WM. With WM, the difference between a REG and a DIFF estimate of eSE is less than 2 percent and unimportant. With B2, the REG estimates of errors are greater than the DIFF estimates, but the difference decreased with increasing sample size from 6 percent with n = 200 to 3 percent with n = 400. The most important differences between REG and DIFF were located with RB, but here too, the differences also decreased with increasing sample size (from 29 percent with n = 200 to 8 percent with n = 400).

The empirical (observed) standard errors (oSE) were, on average (across sample sizes), greatest for WM, approximately 12 percent smaller for B2, and 18 percent smaller for RB (Table 1). Observed REG errors were, as expected from the analyses of the means, very similar to the DIFF estimates.

With the WM model, the REG and DIFF analytical and empirical estimates of standard errors were within a few percentage points (1–4) of each other. With B2, both REG and DIFF underestimated the empirical errors when sample sizes were 200 and 300. The underestimation for these two sample sizes was 4 percent with the REG estimator and 10 percent for DIFF with n = 200. Corresponding results for n = 300 were 4 percent and 7 percent. With the largest sample size, the underestimation was trivial (less than 0.5 percent) with REG but remained high for DIFF (21 percent).

The achieved coverage of nominal 95 percent normal confidence intervals with the WM was, for both REG and DIFF estimators, between 0.94 and 0.95 (Table 1). With a Monte Carlo error (Koehler et al. 2009) of 0.008, we failed to reject the null hypothesis of a coverage equal to the nominal 0.95. With B2, the REG coverage was 0.93–0.94 and 0.92–0.93 for DIFF. With a coverage of 0.93 or less, we rejected the null hypothesis of a coverage of 0.95 at the 5 percent level. Coverage obtained with the RB model and the REG estimator was deficient in all cases (0.90–0.92) and significantly worse with the DIFF estimator (0.81–0.88).

Stand-level MB estimates of relative bias in the WM, B2, and RB estimates of mean VOL were highly variable (Figure 2). When expressed as a percentage of the mean stand volume, the average bias with n = 300, was –4 percent for WM, –10 percent for B2, and 0.4 percent for RB. These averages were practically the same with n = 200 and n = 400. RB achieved—with each sample size—an interquartile range (IQR) of relative bias of 24 percent, much lower than the IQR of 52 percent with WM, and 66 percent with B2.

Given appreciable differences in bias of WM, B2, and RB estimates of stand mean stem volume density, we report on observed (oRMSE) and expected (eRMSE) root mean squared errors in estimates of stand means. With WM, the oRMSE was 159 m^3 ha^{-1} (39 percent of overall mean) with n = 300, 157 m^3 ha^{-1} with n = 300, and 155 m^3 ha^{-1} with n = 400. The eRMSEs were consistently larger (14–21 percent) across all stands and strongly correlated with the oRMSEs (>0.9). Results with B2 were disappointing with both oRMSEs and eRMSEs, being approximately 20 percent greater than corresponding WM results. Only in approximately 50 stands out of 112 were the oRMSE and eRMSE slightly smaller with B2 than with WM. In contrast, with the RB model, the oRMSEs and eRMSEs were smaller in 91 out of 112 stands than with WM. The differences (WM – B2) in oRMSEs ranged from 19 percent (n = 200) to 32 percent (n = 400), whereas the differences in eRMSEs varied from 28 percent (n = 200) to 34 percent (n = 400). Again, the correlation between oRMSEs and eRMSEs was strong (>0.9). Kernel-based probability density distributions of WM, B2, and RB stand-specific averages (over 1,000 replications) of oRMSEs and eRMSEs are shown exemplarily with n = 300 in Figure 3. Distributions for n = 200 and n = 400 were similar (not shown). In the case of RB but not B2, the variance

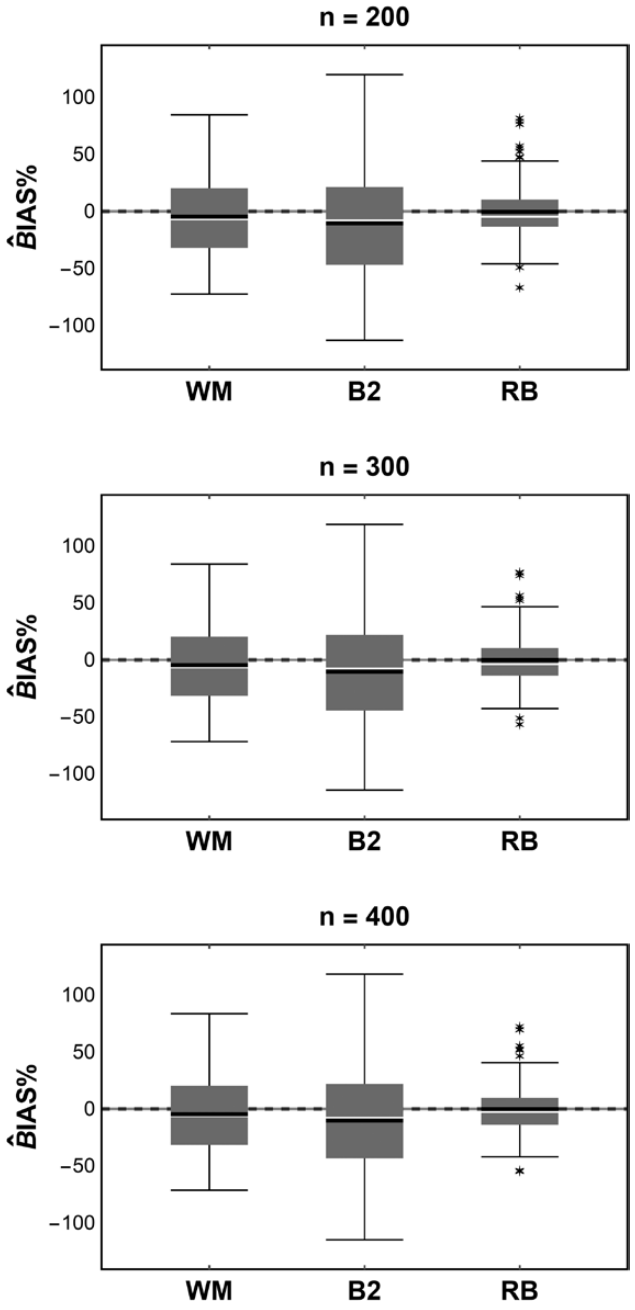

Figure 2. Stand-level distribution of relative bias (true minus predicted) as a percentage of the overall mean stem volume density. The shaded boxes cover the interquartile range, and the whiskers cover 95 percent, i.e., approx. 106 stands. The average relative bias for a model is indicated with a black line. Outliers are indicated by asterisks.

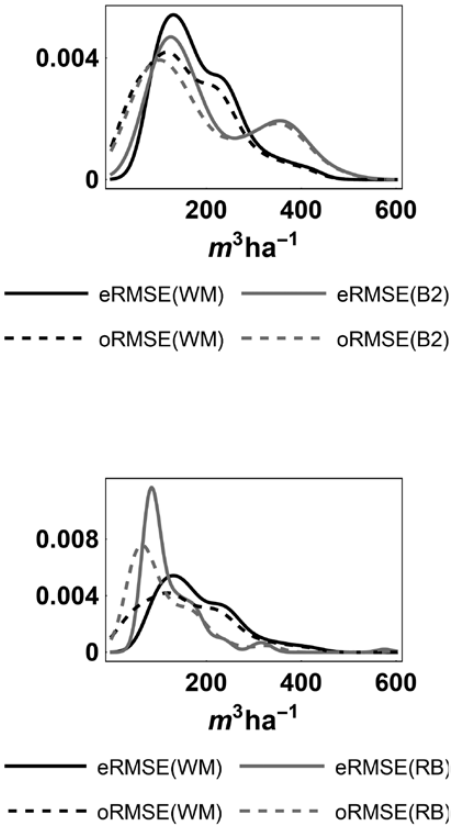

Figure 3. Kernel smoothed distributions of the observed (oRMSE) and expected (eRMSE) root mean squared error of a stand mean.

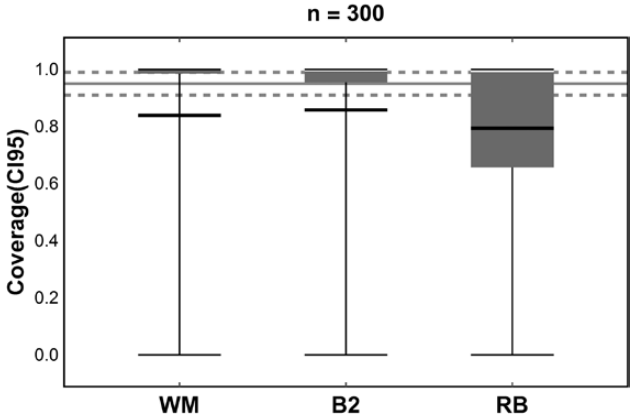

Figure 4. Achieved coverage of 95 percent confidence intervals of an hydrological unit codes forest stand mean of volume density by models WM, B2, and RB. The shaded boxes cover the interquartile range, and the whiskers cover 95 percent, i.e., approx. 106 stands. The average coverage is indicated for each model with a horizontal black line. The gray horizontal line indicates the target coverage of 0.95, and the dashed lines are at 0.91 and 0.99, respectively. Outliers are marked with asterisks.

reduction seen at the population level was even greater at the stand-level. With B2, we actually observed a net increase in variance.

With a sample size of 200, the relative frequency of 95 percent confidence intervals for a stand mean that include the actual stand mean of VOL (i.e., coverage) was, on average, 0.70 for the WM model, 0.59 for the B2 model, and 0.83 for the RB model (Figure 4). The fraction of stands with a coverage of 0.90 (considered as poor) or less with n = 200 was 0.61 for WM, 0.48 for B2, and 63 for RB. An increase in sample size to 300 or 400 lowered coverage because of the combination of a more or less constant bias and a smaller estimate of error. The lowering was most pronounced in WM (0.08 per increase of 100 in sample size) and B2 (0.05 per increase of 100 in sample size), and least in RB (0.02 per increase of 100 in sample size).

BI Data from Baden-Württemberg.

MA estimates for the population-level were underestimating the empirical mean VOL of 432.41 m^3 ha^{-1} obtained from all 770 BI plots in the study area (Table 2). Analytical mean estimates were in the same order of magnitude for all three models (WM, B2, RB) and both types of estimators (REG and DIFF), ranging between 413.5 m^3 ha^{-1} and 420.3 m^3 ha^{-1}. For B2, the DIFF mean VOL (415.7 m^3 ha^{-1}) was slightly lower than the REG mean VOL (420.3 m^3 ha^{-1}), whereas, in contrast, the DIFF mean VOL (416.7 m^3 ha^{-1}) was slightly increased compared to the REG mean VOL (413.5 m^3 ha^{-1}) for RB. When comparing the respective analytical standard errors, it appeared that all of them were smaller than, or at most equal to, the direct estimate of the standard error of VOL, 8.35 m^3 ha^{-1}. The largest REG error was for WM (8.3 m^3 ha^{-1}), followed by B2 (7.4 m^3 ha^{-1}) and RB (6.1 m^3 ha^{-1}). REG results indicated that there was information about VOL in VolnDSM and ELEV not captured with the linear WM. In contrast, the DIFF errors differed only marginally for the three different models (5.6–5.7 m^3 ha^{-1}), potentially underestimating the variance and also not indicating a potential improvement of the linear WM by using nonlinear terms for VolnDSM and ELEV. According to the 95 percent confidence intervals, only the REG estimates from WM and B2 included the empirical (field sample) mean of VOL. In particular, no DIFF-based confidence interval contained the empirical mean VOL.

Stand-level MB estimates of volume density and variances in the 862 forest stands (domains) are captured in Figure 5a–c. Figure 5a displays the kernel density distributions of stand-level estimates of VOL with WM, B2, and RB. A distinction is made between stands with and without BI plots, i.e., with and without information from terrestrial data for reasons given next. Forest stands without terrestrial information—for which the regression-synthetic estimator applies (Rao and Molina 2015, 3.2.2)—have a wider distribution of VOL and a lower median and mean value than stands with terrestrial information. The kernel density distributions in Figure 5b of MB stand-level variances of mean VOL also show a different pattern for stands with and without BI plots. The variances for stands without terrestrial information have a wider distribution than variances for stands with terrestrial information (BI plots). Furthermore, it becomes apparent that in general, RB variances of a stand mean tend to be smaller than counterparts obtained with WM or B2.

The B2 and RB models were expected to capture significant nonlinear departures from the linear WM and to provide improved stand-level estimates by extension. We have no direct means of ascertaining this prospect with the BI data. Instead, we investigated the change in a stand-level estimate of the mean VOL density when switching the model from WM to either B2 or RB. Accordingly, we saw that RB estimates deviated slightly more from WM estimates than did the B2 estimates. Thus, B2 estimates were, on average, closer to the WM

Table 2. Estimates of mean stem volume density in the Betriebsinventur data, associated eSE, and CI_{95}.

Statistic	Estimator	Working model	Second-order model	Radial basis model
Mean	REG	416.4	420.3	413.5
	DIFF	416.4	415.7	416.7
eSE	REG	8.3	7.4	6.1
	DIFF	5.7	5.6	5.6
CI_{95}	REG	[400.0; 432.7]	[405.8; 434.9]	[401.6; 425.4]
	DIFF	[405.2; 427.5]	[404.1; 426.2]	[405.8; 427.7]

Note: The empirical mean of volume density based on all 770 Betriebsinventur plots is 432.4 m^3 ha^{-1}. CI_{95}, 95 percent confidence intervals for the mean; DIFF, difference estimator; eSE, estimated (analytical) standard error; REG, regression estimator.

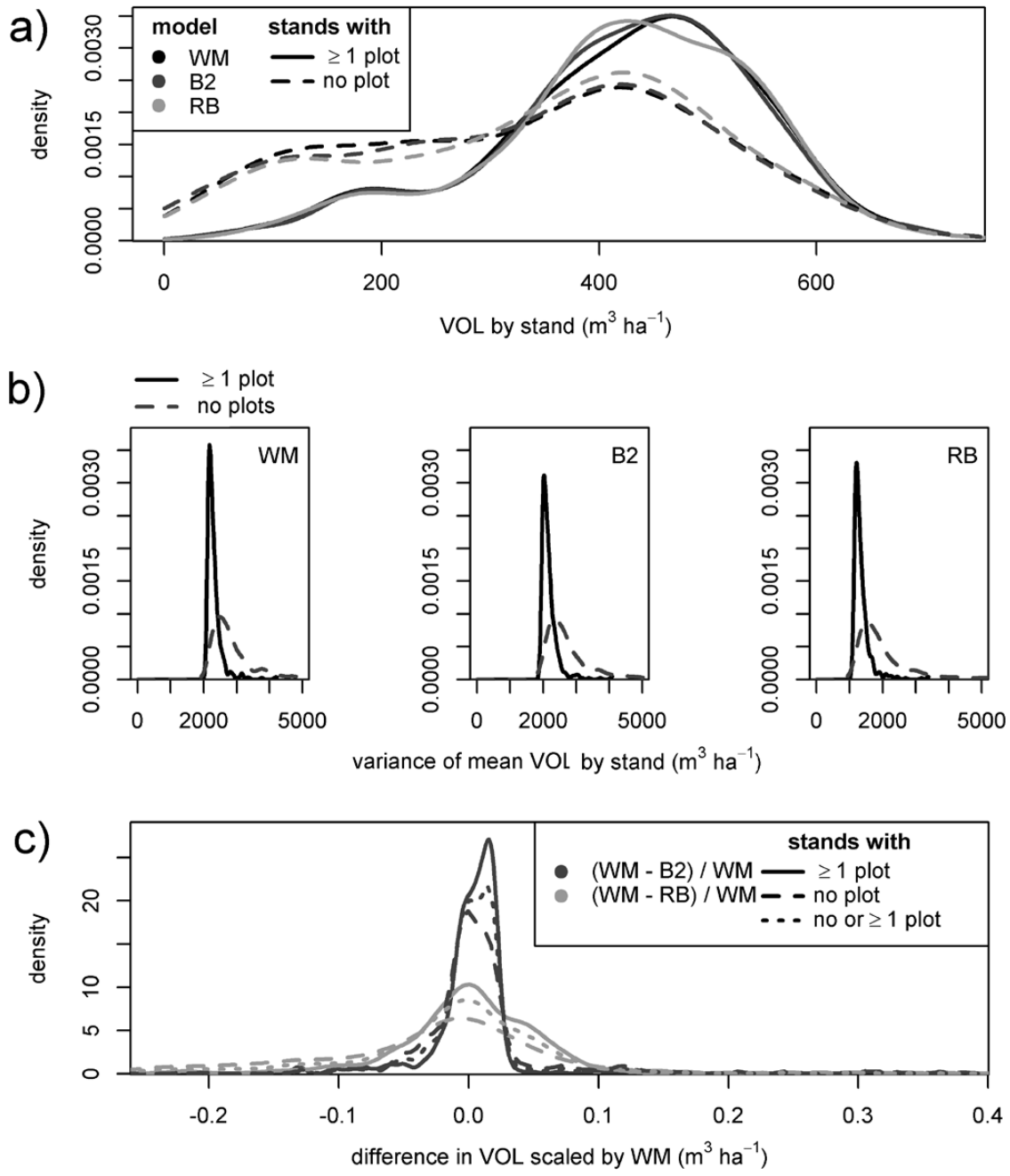

Figure 5. (a) Kernel density plots displaying the mean volume estimates per stand corresponding to all three methods; (b) kernel density plots for the variance of mean volume per stand; (c) kernel density plot of difference between VOL estimates of WM and B2 (dark gray), and RB (light gray), scaled by the VOL estimate of WM per stand. A signature distinction is made between stands with no or at least one BI plot, i.e., information from terrestrial data.

estimates than estimates from RB. Both the B2 and RB distributions of deviations from the WM results resembled a (negligibly left-skewed) normal distribution. As already indicated, the respective distribution for B2 was narrower, e.g., having a smaller variance, than for RB. The mean relative difference in mean VOL between WM and B2 was 1.5 percent, with 95 percent of the differences located between –19 and +22 percent (Figure 5c). The corresponding result for RB was –2 percent with 95 percent of the differences located between –23 and +19 percent. As expected, a separation of the deviations according to whether terrestrial stand-specific inventory information on VOL was available or not showed that the distributions of the scaled differences were wider for stands without BI plots. This behavior was however not as distinct as in Figure 5a and b.

Discussion

At first glance, the extension of a linear WM by a set of basis functions to capture possible nonlinear effects and interactions in auxiliary variables may seem both straightforward and attractive for a design-based population-level inference and a model-based inference at the domain level (Breidt et al. 2007, Opsomer et al. 2007, Cicchitelli and Montanari 2012, Breidt and Opsomer 2017, Wagner et al. 2017). However, when models are fitted to sample data (i.e., the model is "internal")—a common scenario in forest inventories (for examples, see Corona et al. 2014, Mandallaz 2014, Ståhl et al. 2016)—our example with the artificial population indicated that a small bias paired with an important reduction in variance is limited to designs calling for a field sampling with more than (approximately) 5 plots per hectare. With these larger sample sizes, tangible reductions in variance are possible at both the population and domain level with a careful choice of basis functions (cf. results for the RB functions, and for examples, see Opsomer et al. 2008, Finley et al. 2017, Wagner et al. 2017). Yet, within a design-based framework of inference, the model structure has to be defined before the sample is observed (Särndal et al. 1992, ch. 6.7). Hence, attempts to optimize the choice of basis functions, the number and placement of knots, and the auxiliary variables with purported nonlinear effects were not an option in our study.

An analyst, in pursuit of a potential variance reduction with semiparametric modeling within a design-based framework of inference, is therefore faced with a suite of difficult decisions that cannot be resolved by trial and error or optimization. Past experience, subject knowledge, and statistical expertise become key to a successful implementation. For a subsequent model-based domain-level inference, an optimization may be pursued—but this option was considered outside the scope of this study.

In forest inventories, one can make an argument for capturing spatial effects in auxiliary variables (Lappi 2001, Finley et al. 2011). This can be done with a variety of methods, for example, spatial regression (Huque et al. 2016), rule-based nonparametric imputations (Temesgen and Ver Hoef 2014), geo-statistical methods (Mandallaz 2000, Meng et al. 2009), and radial splines (Kato et al. 2009, Rocha and Dias 2019). We saw that significant spatial effects and interactions between variables of spatial location (LAT, LON) could be captured by radial splines, but also that one would have to contend with a risk of underestimating variance, with the REG and in particular with the DIFF estimator. We consider it unlikely that any of the alternatives to the RB would fare better. This is an area in need of further investigation.

With internal nonlinear models, the choice of a design-based estimator of variance becomes important. The DIFF estimator has become popular because the variance is (design-consistently) computed directly from the empirical residuals regardless of the model form (Breidt et al. 2007, Baffetta et al. 2009, Massey et al. 2014, Saarela et al. 2015). Our simulations confirmed that the DIFF estimator of variance is prone to underestimate the actual (observed) variance and that the magnitude of underestimation depends on the intrinsic curvature of the basis functions (see also Massey and Mandallaz 2015, Kangas et al. 2016). The proposed REG estimator of variance employs weighted residuals that calibrate the sample estimates of the auxiliary means to the actual (known) means (Fuller 2011, p. 104). Our simulations suggest that the REG estimator of variance also underestimates the actual variance but to a lesser degree than the DIFF estimator of variance. Application to the BI data further supports the finding from the simulations that the DIFF estimator of variance is lower than the REG estimator of variance. Despite computational complexity, and the triggering of an SVD to fix problems of negative weights, we consider REG a better estimator of variance than DIFF for semiparametric internal models.

The practical consequence of underestimating variance is an increase in the probability that a computed confidence interval does not include (cover) the actual value of an estimated parameter (Rao and Hidiroglou 2003). If it is important to keep the population-level coverage to within 0.01–0.02 of the nominal target, a linear WM would be the choice. However, for a model-based domain-level inference without access to design-consistent estimators of important domain effects—as predicated by our SI design (Magnussen 2018)—a good choice of basis functions can substantially improve otherwise-poor coverage with a linear WM. Notwithstanding, the coverage will, for many domains, still be poor until the sampling design is changed to accommodate a design-consistent estimator of domain effects (Magnussen and Breidenbach 2017).

Appendix A

HUC Forest. The HUC forest is a simulated population composed of 21,025 equal area square units organized to 112 spatially compact managed forest stands (domains). The area of a unit is 706.86 m^2, i.e., equal to the area of a circular fixed area forest inventory sample plot with a radius of 15 m. Thus, the total area of the HUC forest is 1,486.2 hectares. The spatial location, extent, and unit elevation above sea level of the 112 stands were adapted from 112 hydrological basin units in the northeastern United States (Stoddard et al. 2005) and modified to emulate a forested landscape. In particular, the original within-basin variation in elevation was reduced by a factor of 15. HUC is an acronym for hydrological unit code. The same units were used by Opsomer et al. (2008) in a study on nonparametric small area estimation with penalized spline regression.

The size of a stand varies from 0.8 to 43.2 hectares (viz. 12–610 units) with a mean of 13.3 hectares (188 units). One-fourth of the stands were smaller than 6.8 hectares, and one-fourth were greater than 18.2 hectares. Elevation varied from 9 to 657 m with a mean of 239 m. Elevation quartiles (25 percent and 75 percent) were 94 and 369 m, respectively.

The study variable of interest is per unit area stem volume (VOL; unit: $m^3\ ha^{-1}$). Unit-level auxiliary variables correlated with

VOL and available for modeling are: (1) elevation (ELEV; unit: m); (2) longitude (LON °W; unit: degree), and latitude (LAT °N; unit: degree) of a unit centroid; (3) the unit mean CH (unit: m) derived from a simulated surface of presumed vegetation heights; and (4) the standard deviation of canopy heights within a unit (sCH; unit: m).

Simulation of unit-level values of VOL, CH, and sCH was with emphasis on generating realistic data. Only a brief outline of the simulations follows. Stand means of VOL were simulated in seven steps: (1) an SI (viz. the height of dominant trees at age 100 years) expressed as a function of ELEV plus a random deviation; (2) a stand age (*A*; unit: years) expressed as a random number between 0 and 100 plus a random deviation determined by ELEV; (3) a mean dominant tree height (DHT; unit: m) expressed as a function of SI plus a random stand effect; (4) a within-stand standard deviation of dominant tree height (sDHT; unit: m) plus a random stand effect; (5) a stand stem density (*N*; unit: stems ha^{-1}) plus a random stand effect; (6) a mean stem diameter at breast height (dbh) at a reference height of 1.3 m (unit: cm); and (7) a VOL value determined as a function of *N*, DHT, dbh, and SI plus a random stand effect. Stand effects were generated by draws from a multivariate Copula distribution (Fischer 2010) with both normal and uniform marginal distributions.

After simulating stand means of VOL, the stand means of CH and sCH were generated. CH was cast as a function of DHT, sDHT, dbh, SI plus a random stand effect, sCH as a function of sDHT, and CH plus a random stand effect. Random stand effects were random draws from a multivariate Copula distribution with an anticipated correlation structure and scaled to a target value of the among-stand coefficient of variation of approximately 85 percent for VOL, 54 percent for CH, and 22 percent for sCH. Within-stand unit-level values of VOL, CH, and sCH were drawn from a scaled version of the Copula distribution. The scaling was to a target within-stand coefficient of variation of approximately 8 percent for VOL, 7 percent for CH, and 12 percent for sCH.

The above simulations created a finite fixed area population with a mean unit-level VOL of 406 m^3 ha^{-1} (min = 0 m^3 ha^{-1}, max = 1,000 m^3 ha^{-1}) and a unit-level standard deviation of 369 m^3 ha^{-1}. Maps of the spatial distribution of VOL, CH, and sCH are shown in Figure 6 (top right, bottom left, and bottom right). A histogram of stand mean volume is shown in Figure 7.

With an elevation of less than 400 m, there was no clear relation between elevation and VOL m^3 ha^{-1}, but at greater altitudes VOL never exceeded 400 m^3 ha^{-1}. The correlation between CH and VOL was positive for CH less than approximately 20 m, but nearly zero for CH > 20 m. The influence of sCH on VOL was complex. When sCH was less than 2 m, VOL was less than 400 m^3 ha^{-1}. At larger values of sCH, the value of sCH had no obvious bearing on VOL.

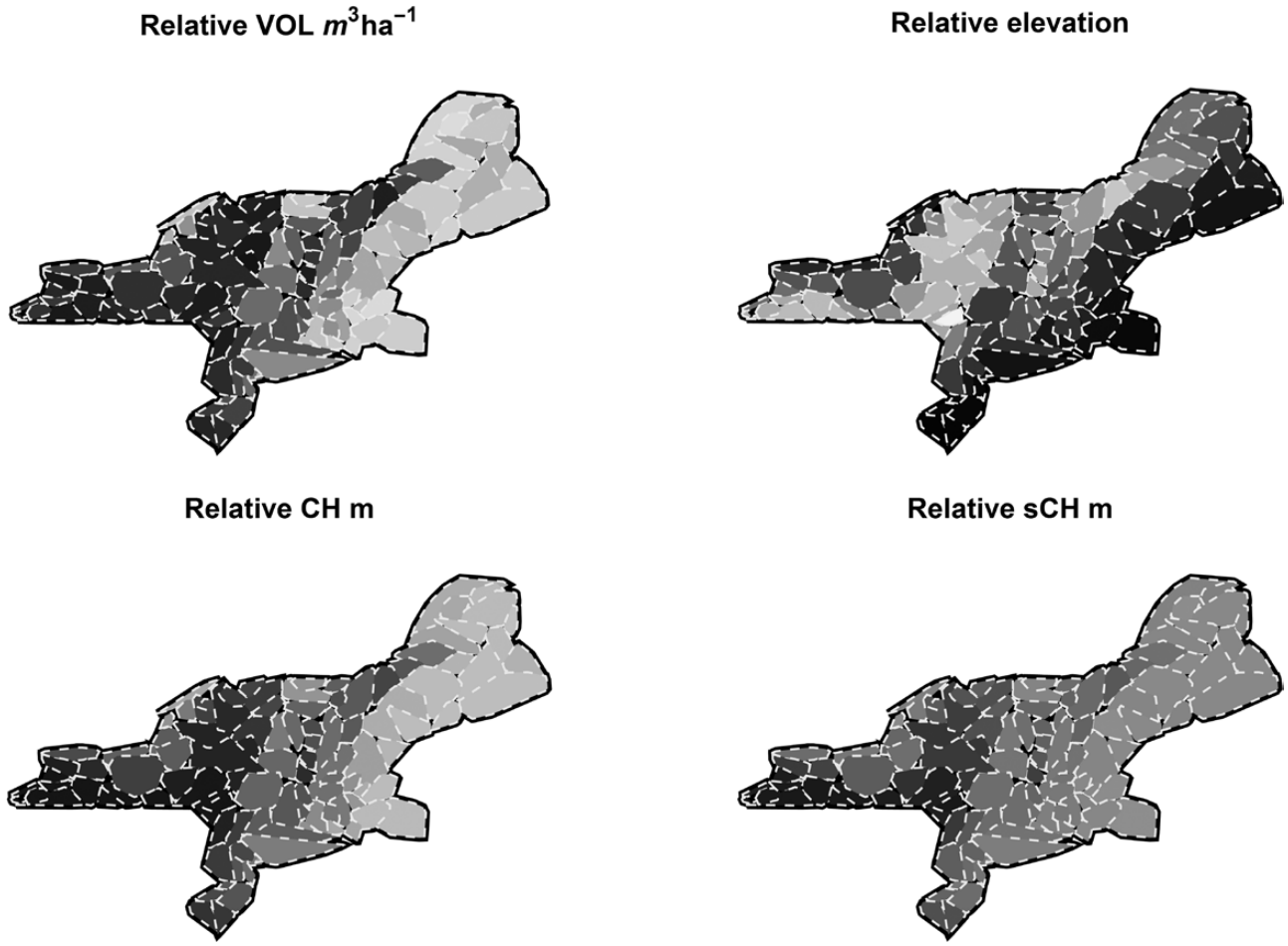

Figure 6. Stand map of relative elevation (top left), per unit area stem volume (top right), canopy height (bottom left), and standard deviation of canopy height (bottom right). Values increase from black to white. Stand boundaries are indicated by dashed lines.

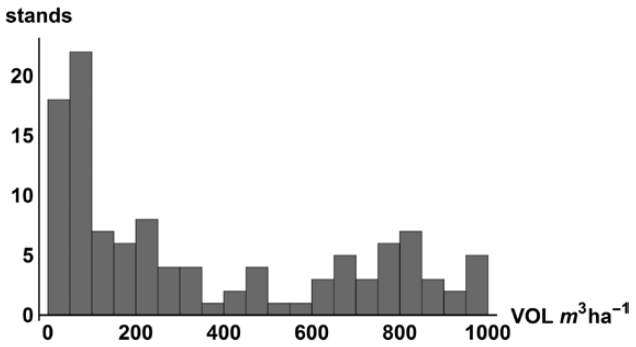

Figure 7. Histogram of stand-level stem volume per unit area in the hydrological unit codes forest.

Appendix B

BI Data from Baden-Württemberg. The considered area in the state forest of "Breisgau-Hochschwarzwald" with image flight data from 2015 is located between 47.784°N and 48.120°N, and 7.532°E and 8.005°E. For the case study, we focused on the subarea located between 47.790°N and 47.955°N, and 7.746°E and 8.008°E. Plots of the BI of Baden-Württemberg are arranged in a systematic grid of 100 × 200 m. For each BI plot, data are collected for single trees in concentric circles. The volume is calculated by means of taper functions requiring the tree attributes "species," "lower diameter" (dbh), "upper diameter," and "height." However, the upper diameter is not measured in the field but estimated based on species-specific form factors derived from volume tables (so-called "volume-table equivalent taper").

A large size digital aerial matrix camera (UltraCam Eagle) with four spectral bands (red [R], green [G], blue [B], and near-infrared [NIR]) and a focal length of 100.5 mm was used during the image flights in 2015. The generated digital aerial stereo images are characterized by a nominal ground resolution of 20 cm, forward overlap of 70 percent, and side overlap of 40 percent. LGL further provided a high-quality DTM with 1-m resolution, being derived from airborne laser scanning data collected between 2001 and 2004, with an approximate point density of 0.8 points per square meter. LGL reported the nominal height accuracy as 0.5 m or better.

The software SURE of nFrames was used to generate a high-resolution DSM point cloud (0.4 m) from the stereo images in a dense image matching process. The filtered point clouds served as a basis to generate a canopy height model, whereas the software LAStools (van Rees 2013) was used to derive a raster-DSM (spatial resolution of 1 m; equivalent to the resolution of the DTM) from each point cloud: within the planimetric pixel extent (1 m^2), the elevation of the highest point was used to the determine each DSM pixel value. If no matching points were available, pixel values were calculated via Triangular Irregular Network streaming (Isenburg et al. 2006). The canopy height models (1 m^2 resolution) were obtained by subtracting the DTM from the photogrammetric DSMs.

Endnote

1. FVA Geobasisdaten © Landesamt für Geoinformation und Landentwicklung Baden-Württemberg, http://www.lgl-bw.de/, Az.: 2851.9-1/19

Literature Cited

Baffetta, F., L. Fattorini, S. Franceschii, and P. Corona. 2009. Design-based approach to the kNN technique for coupling field and remotely sensed data in forest surveys. *Remote Sens. Environ*. 113(3): 463–475.

Bia, M., and P. Van Kerm. 2014. Space-filling location selection. *Stata J.* 13(3):605–622.

Boer, E.P., K.M. de Beurs, and A.D. Hartkamp. 2001. Kriging and thin plate splines for mapping climate variables. *Int. J. Appl. Earth Obs. Geoinf.* 3(2):146–154.

Breidt, F.J., and J.D. Opsomer. 2009. Nonparametric and semiparametric estimation in complex surveys. P. 103–119 in *Handbook of statistics: Sample surveys, inference, and analysis,* Rao, C.R. (ed.). Elsevier, Dordrecht.

Breidt, F.J., and J.D. Opsomer. 2017. Model-assisted survey estimation with modern prediction techniques. *Stat. Sci*. 32(2):190–205.

Breidt, F.J., J.D. Opsomer, A.A. Johnson, and M.G. Ranalli. 2007. Semiparametric model-assisted estimation for natural resource surveys. *Surv. Methodol*. 33(1):35–44.

Buhmann, M.D. 2003. *Radial basis functions: Theory and implementations*. Cambridge University Press, Cambridge.

Carter, C., and G. Eagleson. 1992. A comparison of variance estimators in nonparametric regression. *J. R. Stat. Soc. Series B. Stat. Methodol.* 54(3):773–780.

Chambers, R.L., and R.G. Clark. 2012. *An introduction to model-based survey sampling with applications*. Oxford University Press, New York. 265 p.

Chilès, J.P., and P. Delfiner. 1999. *Geostatistics: Modeling spatial uncertainty*. Wiley, New York. 695 p.

Cicchitelli, G., and G.E. Montanari. 2012. Model-assisted estimation of a spatial population mean. *Int. Stat. Rev*. 80(1):111–126.

Corona, P., L. Fattorini, S. Franceschi, G. Chirici, F. Maselli, and L. Secondi. 2014. Mapping by spatial predictors exploiting remotely sensed and ground data: A comparative design-based perspective. *Remote Sens. Environ.* 152:29–37.

Draper, N.R., and H. Smith. 1998. *Applied regression analysis*. Wiley, New York. 736 p.

Fahrmeir, L., T. Kneib, S. Lang, and B. Marx. 2013. *Regression: Models, methods and applications*. Springer, New York. 698 p.

Finley, A.O., S. Banerjee, and D.W. MacFarlane. 2011. A hierarchical model for quantifying forest variables over large heterogeneous landscapes with uncertain forest areas. *J. Am. Stat. Assoc*. 106(493):31–48.

Finley, A.O., S. Banerjee, Y. Zhou, B.D. Cook, and C. Babcock. 2017. Joint hierarchical models for sparsely sampled high-dimensional LiDAR and forest variables. *Remote Sens. Environ.* 190: 149–161.

Fischer, M. 2010. Multivariate copulae. P. 19–36 in *Dependence modeling*, Kurowicka, D., and H. Joe (eds.). World Scientific, Singapore.

Fuller, W.A. 2011. *Sampling statistics*. Wiley, New York. 454 p.

Gallant, A.R. 1987. *Nonlinear statistical methods*. Wiley, New York. 610 p.

Goerndt, M.E., V.J. Monleon, and H. Temesgen. 2013. Small-area estimation of county-level forest attributes using ground data and remote sensed auxiliary information. *For. Sci*. 59(5):536–548.

Goga, C., and A. Ruiz-Gazen. 2014. Efficient estimation of non-linear finite population parameters by using non-parametrics. *J. R. Stat. Soc. Series B. Stat. Methodol.* 76(1):113–140.

Golub, G.H., and C.F. Van Loan. 2012. *Matrix computations*. JHU Press, Baltimore. 784 p.

Huque, M.H., H.D. Bondell, R.J. Carroll, and L.M. Ryan. 2016. Spatial regression with covariate measurement error: A semiparametric approach. *Biometrics* 72(3):678–686.

Isenburg, M., Y. Liu, J. Shewchuk, J. Snoeyink, and T. Thirion. 2006. Generating raster DEM from mass points via TIN streaming. P. 186–198 in *International conference on geographic information science.* Springer.

Johnson, A.A., F.J. Breidt, and J.D. Opsomer. 2008. Estimating distribution functions from survey data using nonparametric regression. *J. Stat. Theory Pract.* 2(3):419–431.

Johnson, C.R., K. Okubo, and R. Reams. 2001. Uniqueness of matrix square roots and an application. *Linear Algebra Appl.* (323):51–60.

Kangas, A., M. Myllymäki, T. Gobakken, and E. Næsset. 2016. Model-assisted forest inventory with parametric, semiparametric, and nonparametric models. *Can. J. For. Res.* 46(6):855–868.

Kato, A., L.M. Moskal, P. Schiess, M.E. Swanson, D. Calhuon, and W. Stuetzle. 2009. Capturing tree crown information through implicit surface reconstruction using airborne lidar data. *Remote Sens. Environ*. 113:1148–1162.

Koehler, E., E. Brown, and J.-P.A. Haneuse. 2009. On the assessment of Monte Carlo error in simulation-based statistical analyses. *Am. Stat*. 63(2):155–162.

Kublin, E., J. Breidenbach, and G. Kändler. 2013. A flexible stem taper and volume prediction method based on mixed-effects B-spline regression. *Eur. J. For. Res*. 132(5–6):983–997.

Lappi, J. 2001. Forest inventory of small areas combining the calibration estimator and a spatial model. *Can. J. For. Res*. 31:1551–1560.

Lehtonen, R., C.-E. Särndal, and A. Veijanen. 2005. Does the model matter? Comparing model-assisted and model-dependent estimators of class frequencies for domains. *Statist. Transit.* 7(3):649–673.

Lehtonen, R., and A. Veijanen. 2009. Design-based methods of estimation for domains and small areas. P. 219–249 in *Handbook of statistics: Sample surveys, inference, and analysis,* Rao, C.R. (ed.). Elsevier, Dordrecht.

Lister, A., and C. Scott. 2009. Use of space-filling curves to select sample locations in natural resource monitoring studies. *Environ. Monit. Assess.* 149(1):71–80.

Magnussen, S. 2018. An estimation strategy to protect against overestimating precision in a LiDAR-based prediction of a stand mean. *J. For. Sci.* 64(12):497–505.

Magnussen, S., and J. Breidenbach. 2017. Model-dependent forest stand-level inference with and without estimates of stand-effects. *Forest Oxf.* 90(5):675–685.

Mandallaz, D. 2000. Estimation of the spatial covariance in Universal Kriging: Application to forest inventory. *Environ. Ecol. Stat*. 7(3): 263–284.

Mandallaz, D. 2008. *Sampling techniques for forest inventories*. Chapman & Hall, Boca Raton, FL. 251 p.

Mandallaz, D. 2014. *A design-based Monte-Carlo approach to kernel regression estimators in two-phase forest inventories.* ETH, Zurich. 23 p.

Mandallaz, D., J. Breschan, and A. Hill. 2013. New regression estimators in forest inventories with two-phase sampling and partially exhaustive information: A design-based Monte Carlo approach with applications to small-area estimation. *Can. J. For. Res*. 43(11):1023–1031.

Massey, A., and D. Mandallaz. 2015. Comparison of classical, kernel-based, and nearest neighbors regression estimators using the design-based Monte Carlo approach for two-phase forest inventories. *Can. J. For. Res*. 45(11):1480–1488.

Massey, A., D. Mandallaz, and A. Lanz. 2014. Integrating remote sensing and past inventory data under the new annual design of the Swiss National Forest Inventory using three-phase design-based regression estimation. *Can. J. For. Res*. 44:1177–1186.

McConville, K., and F. Breidt. 2013. Survey design asymptotics for the model-assisted penalised spline regression estimator. *J. Nonparametr. Stat*. 25(3):745–763.

McConville, K.S., F.J. Breidt, T.C.M. Lee, and G.G. Moisen. 2017. Model-assisted survey regression estimation with the lasso. *J. Surv. Statist. Meth*. 5(2):131–158.

McRoberts, R.E., E. Næsset, and T. Gobakken. 2013. Inference for lidar-assisted estimation of forest growing stock volume. *Remote Sens. Environ*. 128:268–275.

McRoberts, R.E., E. Næsset, T. Gobakken, G. Chirici, S. Condés, Z. Hou, S. Saarela, Q. Chen, G. Ståhl, and B.F. Walters. 2018. Assessing components of the model-based mean square error estimator for remote sensing assisted forest applications. *Can. J. For. Res*. 48(6):642–649.

Meng, Q., C. Cieszewski, and M. Madden. 2009. Large area forest inventory using Landsat ETM+: A geostatistical approach. *ISPRS J. Photogr. Rem. Sens*. 64(1):27–36.

Montanari, G.E., and M.G. Ranalli. 2005. Nonparametric model calibration estimation in survey sampling. *J. Am. Stat. Assoc*. 100(472):1429–1442.

Næsset, E., O.M. Bollandsås, T. Gobakken, T.G. Gregoire, and G. Ståhl. 2013. Model-assisted estimation of change in forest biomass over an 11 year period in a sample survey supported by airborne LiDAR: A case study with post-stratification to provide "activity data". *Remote Sens. Environ*. 128(0):299–314.

Næsset, E., T. Gobakken, S. Solberg, T.G. Gregoire, R. Nelson, G. Ståhl, and D. Weydahl. 2011. Model-assisted regional forest biomass estimation using LiDAR and InSAR as auxiliary data: A case study from a boreal forest area. *Remote Sens. Environ*. 115(12): 3599–3614.

Nothdurft, A. 2013. Spatio-temporal prediction of tree mortality based on long-term sample plots, climate change scenarios and parametric frailty modeling. *For. Ecol. Manag.* 291:43–54.

Opsomer, J.D., F.J. Breidt, G.G. Moisen, and G. Kauermann. 2007. Model-assisted estimation of forest resources with generalized additive models. *J. Am. Stat. Assoc*. 102(478):400–409.

Opsomer, J.D., G. Claeskens, M.G. Ranalli, G. Kauermann, and F. Breidt. 2008. Non-parametric small area estimation using penalized spline regression. *J. R. Stat. Soc. Series B. Stat. Methodol.* 70(1):265–286.

Opsomer, J.D., and C.P. Miller. 2007. Selecting the amount of smoothing in nonparametric regression estimation for complex surveys. *J. Nonparametr. Stat*. 17(5):593–611.

Penner, M., D.G. Pitt, and M.E. Woods. 2013. Parametric vs. nonparametric LiDAR models for operational forest inventory in boreal Ontario. *Can. J. Rem. Sens*. 39(05):426–443.

Pinheiro, J.C., and D.M. Bates. 2000. *Mixed-effects models in S and S-plus*. Springer, New York. 1–528 p.

Poggio, L., and A. Gimona. 2013. Modelling high resolution RS data with the aid of coarse resolution data and ancillary data. *Int. J. Appl. Earth Obs. Geoinf.* 23:360–371.

Ranalli, M.G., F.J. Breidt, and J.D. Opsomer. 2016. Nonparametric regression methods for small area estimation. P. 187–204 in *Analysis of poverty data by small area estimation*. Wiley, New York.

Rao, J., and M. Hidiroglou. 2003. Confidence interval coverage properties for regression estimators in uni-phase and two-phase sampling. *J. Off. Stat.* 19(1):17–30.

Rao, J.N., and I. Molina. 2015. *Small area estimation*. Wiley, New York. 480 p.

Rocha, H., and J. Dias. 2019. Early prediction of durum wheat yield in Spain using radial basis functions interpolation models based on agroclimatic data. *Comput. Electron. Agr.* 157:427–435.

Ruppert, D., M. Wand, and R.J. Carroll. 2003. *Semiparametric regression*. Cambridge University Press, Cambridge. 386 p.

Saarela, S., A. Grafström, G. Ståhl, A. Kangas, M. Holopainen, S. Tuominen, K. Nordkvist, and J. Hyyppä. 2015. Model-assisted estimation of growing stock volume using different combinations of LiDAR and Landsat data as auxiliary information. *Remote Sens. Environ*. 158(1):431–440.

Särndal, C.E., B. Swensson, and J. Wretman. 1992. *Model assisted survey sampling*. Springer, New York. 694 p.

Searle, S.R. 1982. *Matrix algebra useful for statistics*. Wiley, New York. 438 p.

Searle, S.R., G. Casella, and C.E. McCulloch. 1992. *Variance components*. Wiley, New York. 501 p.

Ståhl, G., S. Saarela, S. Schnell, S. Holm, J. Breidenbach, S. Healey, P. Patterson, et al. 2016. Use of models in large-area forest surveys: Comparing model-assisted, model-based and hybrid estimation. *For. Ecosyst.* 3(1):5.

Stoddard, J., D. Peck, A. Olsen, D. Larsen, J. Van Sickle, C. Hawkins, R. Hughes, T. Whittier, G. Lomnicky, and A. Herlihy. 2005. *Environmental monitoring and assessment program (EMAP): Western streams and rivers statistical summary*. US Environmental Protection Agency, Office of Research and Development, Washington, DC.

Temesgen, H., and J.M. Ver Hoef. 2014. Evaluation of the spatial linear model, random forest and gradient nearest-neighbour methods for imputing potential productivity and biomass of the Pacific Northwest forests. *Forestry* cpu036.

Tipton, J., J. Opsomer, and G. Moisen. 2013. Properties of endogenous post-stratified estimation using remote sensing data. *Remote Sens. Environ*. 139:130–137.

Tomppo, E. 2006. The Finnish multi-source national forest inventory—small area estimation and map production. P. 195–224 in *Forest inventory—methodology and applications*, Kangas, A., and M. Maltamo (eds.). Springer, Dordrecht, NL.

van Rees, E. 2013. Rapidlasso: Efficient tools for LiDAR processing. *GeoInformatics* 16(7):14.

Wagner, J., R. Münnich, J. Hill, J. Stoffels, and T. Udelhoven. 2017. Non-parametric small area models using shape-constrained penalized B-splines. *J. R. Stat. Soc. A. Stat.* 180(4):1089–1109.

Wulder, M., N. Coops, A. Hudak, F. Morsdorf, R. Nelson, G. Newnham, and M. Vastaranta. 2013. Status and prospects for LiDAR remote sensing of forested ecosystems. *Can. J. Rem. Sens*. 39(Supp 1):S1–S5.